The Journal of Immunology

RESEARCH ARTICLE | APRIL 15 2014

CCL3 Production by Microglial Cells Modulates Disease Severity in Murine Models of Retinal Degeneration

Hideo Kohno; ... et. al

J Immunol (2014) 192 (8): 3816–3827.
https://doi.org/10.4049/jimmunol.1301738

CCL3 Production by Microglial Cells Modulates Disease Severity in Murine Models of Retinal Degeneration

Hideo Kohno,*,† Tadao Maeda,*,‡ Lindsay Perusek,‡ Eric Pearlman,‡ and Akiko Maeda*,‡

Many degenerative retinal diseases illustrate retinal inflammatory changes that include infiltration of microglia and macrophages into the subretinal space. In this study, we examined the role of chemokines in the *Abca4*$^{-/-}$*Rdh8*$^{-/-}$ mouse model of Stargardt disease and the *Mertk*$^{-/-}$ mouse model of retinitis pigmentosa. PCR array analysis of 84 chemokines and related molecules revealed 84.6-fold elevated expression of *Ccl3* (*MIP-1a*) 24 h after light exposure in *Abca4*$^{-/-}$*Rdh8*$^{-/-}$ mice. Only MIP-1 chemokines, including *Ccl3* and *Ccl4*, displayed peak expression 24 h after light exposure, and peaked earlier than the other chemokines. Secretion of Ccl3 was documented only in microglia, whereas both microglia and retinal pigment epithelium cells produced Ccl2. Exposure of *Cx3Cr1*$^{gfp/\Delta}$*Abca4*$^{-/-}$*Rdh8*$^{-/-}$ mice to intense light resulted in the appearance of *Cx3Cr1*GFP^{+} monocytes in the subretinal space. To address the in vivo role of CCL3 in retinal degeneration, *Ccl3*$^{-/-}$*Abca4*$^{-/-}$*Rdh8*$^{-/-}$ mice and *Ccl3*$^{-/-}$*Mertk*$^{-/-}$ mice were generated. Following intense light exposure, *Ccl3*$^{-/-}$*Abca4*$^{-/-}$*Rdh8*$^{-/-}$ mice displayed persistent retinal inflammation with appearance of Iba-1^{+} cells in the subretinal space, severe photoreceptor cell death, and increased *Ccl4* expression compared with *Abca4*$^{-/-}$*Rdh8*$^{-/-}$ mice. In contrast, *Ccl3*$^{-/-}$*Abca4*$^{-/-}$*Rdh8*$^{-/-}$ mice exhibited a milder retinal inflammation and degeneration than *Abca4*$^{-/-}$*Rdh8*$^{-/-}$ mice did in age-related chronic retinal degeneration under room light conditions. The deficiency of *Ccl3* also attenuated the severity of retinal degeneration in *Mertk*$^{-/-}$ mice. Taken together, our results indicate that Ccl3 has an essential role in regulating the severity of retinal inflammation and degeneration in these mouse models. ***The Journal of Immunology*****, 2014, 192: 3816–3827.**

Clinical and experimental evidence suggests an important role for inflammation in retinal degeneration (1–4). Microglial cells are resident macrophages in the CNS and play a key role in this pathologic inflammatory process (2). Therefore, elucidating the activities and functions of these inflammatory cells is essential in expanding our knowledge of the pathology of retinal degeneration. Understanding the role of chemokines in retinal degeneration is particularly important because they not only dictate the migration of inflammatory cells, they are also potential drivers of retinal degenerative conditions in humans and mice (5, 6).

The visual process is initiated in photoreceptors by activation of rhodopsin through the photoconversion of visual chromophore 11-*cis*-retinal to all-*trans*-retinal. This isomeric conversion initiates a signaling cascade that ultimately propagates the visual stimulus to the brain. To maintain vision, all-*trans*-retinal is recycled for regeneration of 11-*cis*-retinal via the visual cycle, which is a series of biochemical reactions in photoreceptors and in retinal pigment epithelial (RPE) cells (7, 8). Although all-*trans*-retinal is an essential source for regeneration of rhodopsin, delayed clearance of all-*trans*-retinal is closely associated with retinal disorders (9–11). Clearance of all-*trans*-retinal in photoreceptors occurs in two steps: translocation of all-*trans*-retinal from the inside to the outside of photoreceptor outer segment (POS) discs by the ATP-binding cassette transporter 4 (ABCA4) (12) and reduction of all-*trans*-retinal to all-*trans*-retinol in the cytosolic lumen of photoreceptor outer segments by retinol dehydrogenase 8 (RDH8) (13, 14). We previously developed a model of retinal degeneration in mice mediated by all-*trans*-retinal in which *Abca4* and *Rdh8* are deleted (15, 16). This model reproduces many features of human Stargardt- and AMD-like retinal phenotype characterized by lipofuscin accumulation, drusen formation, complement activation, photoreceptor/RPE atrophy, and choroidal neovascularization (16). The uniqueness of this model is that the *Abca4*$^{-/-}$*Rdh8*$^{-/-}$ mouse not only displays age-related chronic degeneration under room light conditions, but also displays acute retinal degeneration when exposed to intense light (15). Our previous study showed that *Abca4*$^{-/-}$*Rdh8*$^{-/-}$ mice exposed to intense light exhibited increases in several proinflammatory molecules (2). However, these increases were transient, and all inflammatory molecules returned to the basal level 7 d after light exposure. Proinflammatory molecules increased in age-related chronic degenerated retinas of *Abca4*$^{-/-}$*Rdh8*$^{-/-}$ mice, but many anti-inflammatory molecules were also shown to increase in these mice. These anti-inflammatory molecules included: complement factor H, a regulator of the complement cascade, Arginase liver (ARG1), a marker of M2 macrophages which possesses anti-inflammatory properties (17), and TGF, β 1 (TGFB), a regulator of the immune cascade. These

*Department of Pharmacology, Case Western Reserve University, Cleveland, OH 44106; †Department of Ophthalmology, The Jikei University School of Medicine, Tokyo 105-8461, Japan; and ‡Department of Ophthalmology and Visual Sciences, Case Western Reserve University, Cleveland, OH 44106

Received for publication July 1, 2013. Accepted for publication February 8, 2014.

This work was supported by funding from the National Institutes of Health (Grants EY022658, EY019031, EY019880, EY021126, and EY11373), the Research to Prevent Blindness Foundation, the Foundation Fighting Blindness, and the Ohio Lions Eye Research Foundation.

Address correspondence and reprint requests to Dr. Akiko Maeda, Department of Ophthalmology and Visual Sciences, Case Western Reserve University, 10900 Euclid Avenue, Cleveland, OH 44106-7286. E-mail address: aam19@case.edu

The online version of this article contains supplemental material.

Abbreviations used in this article: AF, autofluorescence; GFAP, glial fibrillary acidic protein; IHC, immunohistochemistry; ONL, outer nuclear layer; POS, photoreceptor outer segment; RDH8, retinol dehydrogenase 8; RPE, retinal pigment epithelium; SD-OCT, spectral-domain optic coherence tomography; SLO, scanning laser ophthalmoscopy.

findings point to the paradoxical nature of the inflammatory response in *Abca4*$^{-/-}$*Rdh8*$^{-/-}$ mice.

In this study, we present data indicating that CCL3 is a critical regulator of retinal inflammation, which is associated with severity of retinal degeneration.

Materials and Methods

Animals

Abca4$^{-/-}$*Rdh8*$^{-/-}$ mice were generated as described previously, and all mice were genotyped as described previously (16). Only mice with the leucine variation at aa 450 of RPE65 were used. *Rd8* mutation on *Crb1* gene was also assessed (18) and only mice without this mutation were used in this study. *Ccl3*$^{-/-}$, *Ccl2*$^{-/-}$, *Mertk*$^{-/-}$, and *Cx3Cr1*$^{gfp/\Delta}$ mice were obtained from The Jackson Laboratory (Bar Harbor, ME). Genotyping for *Ccl3* was performed with primers; for wild type forward; 5′-ATGAAGGTCTCCACCACTGC-3′, reverse; 5′-AGTCAACGATGAATTGGCG-3′, for mutant forward; 5′-TAAAGCATGCTCCAGACT-3′ and reverse, 5′-CAAAGGCTGCTGGTTTCAAA-3′ (19). Genotyping for *Ccl2* was performed with primers; for wild type forward; 5′- TGACAGTCCCCAGAGTCACA-3′, common reverse; 5′-TCATTGGGATCATCTTGCTG -3′, for mutant forward; 5′-GCCAGAGGCCACTTGTGTAG-3′, for *Mertk* was performed with primers; for wild type forward; 5′-GCTTTAGCCTCCCCAGTAGC-3′, reverse; 5′-GGTCACATGCAAAGCAAATG-3′, for mutant forward; 5′-CGTGGAGAAGGTAGTCGTACATCT-3′ and reverse; 5′-TTTGCCAAGTTCTAATTCCATC-3′, and for *Cx3Cr1* was performed with primers; for wild type, 5′−TCCACGTTCGGTCTGGTGGG-3′ and 5′−GGTTCCTAGTGGAGCTAGGG−3′; and *Cx3cr1*−*GFP* mutant, 5′−GATCACTCTCGGCATGGACG−3′ and 5′−GGTTCCTAGTGGAGCTAGGG−3′ according to the protocol from The Jackson Laboratory. C57BL/6 or littermate control mice were used as WT mice. Equal numbers of males and females were used. All mice were housed in the animal facility at the School of Medicine, Case Western Reserve University, where they were maintained either under complete darkness or in a 12-h light (~10 lx) an 12-h dark cycle environment. Experimental manipulations in the dark were done under dim red light transmitted through a Kodak No. 1 safelight filter (transmittance > 560 nm). All animal procedures and experiments were approved by the Case Western Reserve University Animal Care Committees and conformed to both the recommendations of the American Veterinary Medical Association Panel on Euthanasia and the Association of Research for Vision and Ophthalmology.

Induction of light damage

Mice were dark-adapted for 48 h before exposure to light. Light damage was induced by exposing mice to 10,000 lx of diffuse white fluorescent light (150 W spiral lamp; Commercial Electric, Cleveland, OH) for 30 or 15 min. Before such light exposure, pupils of mice were dilated with a mixture of 0.5% tropicamide and 0.5% phenylephrine hydrochloride (Midorin-P, Santen Pharmaceutical, Osaka, Japan), and after exposure animals were kept in the dark until evaluation.

Histologic analysis

All procedures to make sections for immunohistochemistry (IHC) and light microscopy were performed as described previously (14). The following Abs were used for IHC; rabbit anti-Iba1 Ab (1:400; Wako, Chuo-ku, Osaka, Japan), rabbit anti-Glial Fibrillary Acidic Protein Ab (GFAP; 1:400; Dako, Carpinteria, CA), mouse anti−rhodopsin 1D4 Ab (1:100, gift from Dr. Robert Molday, University of British Columbia, Vancouver, Canada), anti–T cell Ab (anti-CD3; 1: 200, Dako), anti-CD45 Ab (1:200, Abcam, Cambridge, MA), monoclonal anti-mouse neutrophil Ab (NIMP-R14; 1:200, Abcam) and Alexa 488−conjugated peanut agglutinin (PNA; 1:200, Invitrogen). Images of IHC were captured by a confocal microscope (LSM, Carl Zeiss, Thornwood, NY).

Flat-mount RPE preparation for immunostaining

All procedures to make flat-mount RPE were described previously (2). Rabbit anti-ZO-1 Ab (1:200, Invitrogen) was used. Size of RPE cells was measured by LSM image browser (Carl Zeiss, Thornwood, NY).

Scanning laser ophthalmoscopy imaging and ultra-high-resolution spectral domain optical coherence tomography

HRAII (Heidelberg Engineering, Heidelberg,Germany) for scanning laser ophthalmoscopy (SLO) and ultra-high resolution spectral domain optical coherence tomography (SD-OCT; Bioptigen, Research Triangle Park, NC) were used for in vivo imaging of mouse retinas. Mice were anesthetized by i.p. injection of a mixture (20 μl/g body weight) containing ketamine (6 mg/ml) and xylazine (0.44 mg/ml) in 10 mM sodium phosphate, pH 7.2, with 100 mM NaCl. Pupils were dilated with a mixture of 0.5% tropicamide and 0.5% phenylephrine hydrochloride (Midorin-P, Santen Pharmaceutical). Five pictures acquired in the B-scan mode were used to construct each final averaged SD-OCT image. SD-OCT images were scored using our previously established scoring system (20).

Isolation of primary RPE and retinal microglial cells

Primary mouse RPE cells and retinal microglial cells were prepared from 2-wk-old mice. Enucleated eyes were incubated with 2% dispase (Invitrogen) in DMEM (Invitrogen) for 1 h at 37°C, and neural retinas and eyecups were separated under a surgical microscope (ILLUMIN-i; Endure Medical, Cumming, GA). The RPE layer was peeled from eyecups, passed through 70-μm and 40-μm nylon mesh filters (Falcon Plastics, Brookings, SD), and cultured in DMEM containing MEM nonessential amino acids (Invitrogen), penicillin–streptomycin (Invitrogen), 20 mM HEPES, pH 7.0, and 10% FBS. To enrich microglial cells, neural retinas were homogenized and cultured in DMEM containing MEM nonessential amino acids (Invitrogen), penicillin–streptomycin (Invitrogen), 20 mM HEPES, pH 7.0, and 10% FBS for 7 d at 37°C. Adherent cells to the plastic surface were treated with 0.05% trypsin (Invitrogen), and less adhesive cells were collected as microglial cells.

ELISA

Production of Ccl2 and Ccl3 from retinal primary cells was quantified by ELISA kits (Ccl2; MJE00 and Ccl3; MMA00) purchased from R&D systems (Minneapolis, MN) with 50 μl of cell culture supernatants of primary RPE or microglial cells. Concentrated cell lysates were prepared with NP-40 lysis buffer containing 20 mM Tris, pH 8.0, 137 mM NaCl, 10% glycerol, and 1% NP-40. Then protein concentration was measured with a BCA protein assay kit (Pierce, Rockford, IL). Production of Ccl3, Ccl4, and Il-1β was also quantified by ELISA kits from R&D systems (Ccl4; MMB00 and IL-1β; MLB00C) with mouse eyes. Two eyes from one mouse were homogenized in 500 μl of PBS with protease inhibitor cocktails (Roche) by a glass-glass homogenizer. The homogenates (50 μl) were used for the quantification. A single data point was obtained from each mouse (2 eyes).

Fundus fluorescein angiography

Fluorescein Sodium (ANGIOFLUOR; Alliance Pharmaceuticals, Richmond, TX) was diluted in PBS to 25 mg/ml and injected 2.5 mg per 100 μl per mouse via i.p. injection 10 min prior to taking images. Fundus fluorescein angiography was performed by HRAII (Heidelberg Engineering).

Quantitative RT-PCR

All procedures for quantitative RT-PCR were described previously (2). Following primers were used for analyses: *Ccl3* (231 bp), forward 5′- CTGCCCTTGCTGTTCTTCTC-3′, reverse 5′-CTTGGACCCAGGTCTCTTTG-3′; *Ccl4* (196 bp), forward 5′-GCCCTCTCTCTCCTCTTGCT-3′, reverse 5′-GTCTGCCTCTTTTGGTCAGG-3′; *Ccl2* (187 bp), forward 5′-GCTGACCCCAAGAAGGAATG-3′, reverse 5′-GTGCTTGAGGTGGTTGTGGA-3′; *Ccr1* (206 bp), forward 5′-TTCCTCCTCTGGACCCCCTA-3′, reverse 5′-TTGAAACAGCTGCCGAAGGT-3′ ; *Ccr5* (172 bp), forward 5′-GCTGCCTAAACCCTGTCATC-3′, reverse 5′-TCATGTTCTCCTGTGGATCG-3′; *Ccr2* (227 bp), forward 5′-ATTCTCCACACCCTGTTTCG-3′, reverse 5′-ATGCAGCAGTGTGTCATTCC-3′; *Ccl12* (188 bp), forward 5′-CAGTCCTCAGGTATTGGCTGGA-3′, reverse5′-TCCTTGGGGTCAGCACAGAT-3′; *Cxcl10* (154 bp), forward 5′-CCTCATCCTGCTGGGTCTG-3′, reverse 5′-CTCAACACGTGGGCAGGA-3′; *Il1β* (167 bp), forward 5′-CCTGCAGCTGGAGAGTGTGG-3′, reverse 5′-CCAGGAAGACAGGCTTGTGC-3′; *Nox2* (207 bp), forward 5′-TCGAAAACTCCTTGGGTCAG-3′, reverse 5′-TGCAGTGCTATCATCCAAGC-3′; *Arg1* (181 bp) forward 5′- CGCCTTTCTCAAAAGGACAG-3′, reverse 5′- ACAGACCGTGGGTTCTTCAC-3′; *TGF, β 1* (*Tgfb*, 185 bp) forward 5′- TGAGTGGCTGTCTTTTGACG-3′, reverse 5′-GGTTCATGTCATGGATGGTG-3′; *Gapdh* (150 bp), forward 5′-GTGTTCCTACCCCCAATGTG-3′, reverse 5′- AGGAGACAACCTGGTCCTCA-3′. Relative expression of genes was normalized by housekeeping gene *Gapdh*.

Quantitative RT-PCR–based RNA expression analysis

RNA expression analysis was performed by RT^2 Profiler PCR Array System provided by SABiosciences (Frederic, MD). Fold changes were calculated after the data normalized to five housekeeping genes. Total RNA was purified from 16 retinas of 4-wk-old *Abca4*$^{-/-}$*Rdh8*$^{-/-}$ and WT mice at each time point by RiboPure kit (Ambion, Austin, TX).

Data analysis

Data representing the means ± SD for the results of at least three independent experiments were compared by the one-way ANOVA test.

Results

Ccl3 expression shows the greatest increase in the retina of light exposed Abca4$^{-/-}$Rdh8$^{-/-}$ mice

To investigate the involvement of chemokines in light induced acute retinal degeneration of *Abca4*$^{-/-}$*Rdh8*$^{-/-}$ mice, PCR array analysis for 84 different chemokines and related molecules was performed (Table I). Retinas were harvested from *Abca4*$^{-/-}$*Rdh8*$^{-/-}$ and WT mice 24 h and 7 d after light exposure at 10,000 lx for 30 min. Expression levels of dark adapted *Abca4*$^{-/-}$*Rdh8*$^{-/-}$ and WT mice were used as a basal control for light exposed *Abca4*$^{-/-}$*Rdh8*$^{-/-}$ and WT mice, respectively. *Ccl2*, *Ccl3*, *Ccl4*, *Ccl12*, and *Cxcl10* expression increased 10-fold or higher in light exposed *Abca4*$^{-/-}$*Rdh8*$^{-/-}$ mice when compared with dark-adapted mice. *Ccl3* expression at 24 h showed an 84.6-fold increase as the greatest change of all tested genes. Only *Cxcl10* increased 10-fold or higher in light exposed WT mice.

Expression of MIP-1 genes peaks earlier than others do after light treatment in Abca4$^{-/-}$Rdh8$^{-/-}$ mice

To understand the dynamic nature of the expression of these inflammatory markers that showed 10-fold or higher changes, a time course measurement was conducted. The time course analyses using quantitative PCR for chemokines and chemokine receptors (Fig. 1) revealed that only MIP-1 transcripts, including *Ccl3* and *Ccl4*, peaked 24 h after light exposure in *Abca4*$^{-/-}$*Rdh8*$^{-/-}$ mice. In contrast, *Ccl2*, *Cxcl10*, and *Ccl12* had a different temporal profile, which peaked 3 d after light treatment. Light-exposed WT mice did not show a significant increase in these chemokines at either 24 h or 3 d after light exposure. Chemokine receptors were also investigated to determine any changes in expression levels. *Ccr1*, which is a receptor for *Ccl3* and *Ccr2*, which is a receptor of *Ccl2* and *Ccl12*, peaked 3 d after light exposure in *Abca4*$^{-/-}$*Rdh8*$^{-/-}$ mice. *Ccr5*, a receptor for *Ccl3* and *Ccl4* peaked 12 h and continuously increased until 3 d after light exposure in *Abca4*$^{-/-}$*Rdh8*$^{-/-}$ mice.

To determine the likely source of Ccl3 and Ccl2 in the retina, primary cultured RPE cells and microglia were isolated from 2-wk-old *Abca4*$^{-/-}$*Rdh8*$^{-/-}$ mice (2) and coincubated with POS, which activate microglia/macrophages via TLR4 (2), LPS, a ligand of TLR4, and Pam3CSK4, a ligand of TLR1/2. Protein amounts of

Table I. Expression of chemokines and their related molecules in mouse retinas after light exposure

		Abca4$^{-/-}$*Rdh8*$^{-/-}$ mice[a,b]		WT	
	Genes	(24 h)	(7 d)	(24 h)	(7 d)
CC chemokine	***Ccl2***	**30.52**	1.13	−1.40	−2.93
	Ccl3	**84.59**	**27.14**	1.83	−2.09
	Ccl4	**34.29**	6.52	1.41	−4.26
	Ccl5	4.45	3.61	4.68	1.80
	Ccl7	9.56	−2.94	−2.04	−3.12
	Ccl8	−2.60	−3.39	−3.00	−10.26
	Ccl11	−4.13	−9.28	−3.21	−6.49
	Ccl12	**13.57**	1.92	1.73	−3.28
CCR	*Ccr2*	5.95	7.84	−9.32	−25.05
	Ccr3	**29.04**	**31.76**	−1.21	−1.19
	Ccr6	−3.01	−3.39	−1.23	−2.76
	Ccr7	1.62	3.88	−1.51	−1.44
	Ccr10	2.46	3.51	7.62	3.43
CXC chemokine	*Cxcl1*	4.68	−1.36	1.62	−2.93
	Pf4	−5.16	−1.68	−3.55	−3.57
	Cxcl5	7.26	−2.01	8.96	8.53
	Cxcl10	**21.10**	1.73	**13.15**	−2.00
CXCR	*Cxcr5*	3.32	5.09	1.48	1.10
IL	*Il1b*	6.44	1.47	−1.25	1.22
	Il1f6	−3.45	−1.82	−4.06	−2.77
	Il1f8	−15.87	−32.42	2.97	1.22
	Il4	8.88	3.07	4.61	2.97
	Il16	3.01	1.16	−1.74	−2.93
	Il20	−3.76	−3.05	−1.45	−3.79
IL receptor	*Il1r1*	1.69	1.46	1.64	1.61
	Il1r2	−5.14	−6.36	−2.67	−1.77
	Il5ra	4.35	6.16	2.91	2.52
	Il6ra	6.47	1.26	−2.01	−2.21
	Il8rb	4.65	−4.75	−3.21	−2.93
	Il10ra	−1.42	4.06	−1.36	−1.01
Others	*Ifng*	3.58	2.59	−3.21	−2.93
	Tgfb1	1.74	2.63	3.62	3.03
	Itgb2	1.88	4.58	1.00	−1.10
	Spp1	1.56	3.34	−2.51	−2.76
	Tnfrsf1a	5.47	3.14	2.74	1.84
	Bcl6	3.39	1.84	3.28	2.78

Fold changes greater than 3 compared with data obtained from dark adapted mice are presented. The data were normalized to the housekeeping genes (*Gusb*, *Gapdh*, *Actb*, *Hprt1*, and *Hsp90ab1*). Fold changes greater than 10 are presented in bold text. Minus signs (–) indicate reduced expression.

[a]Mice were exposed to 10,000 lx white light for 30 min after 48 h of dark adaptation. Before such light exposure, pupils of mice were dilated. Mice were kept in the dark until evaluations.

[b]RNA was purified from 16 retinas of 4-wk-old mice.

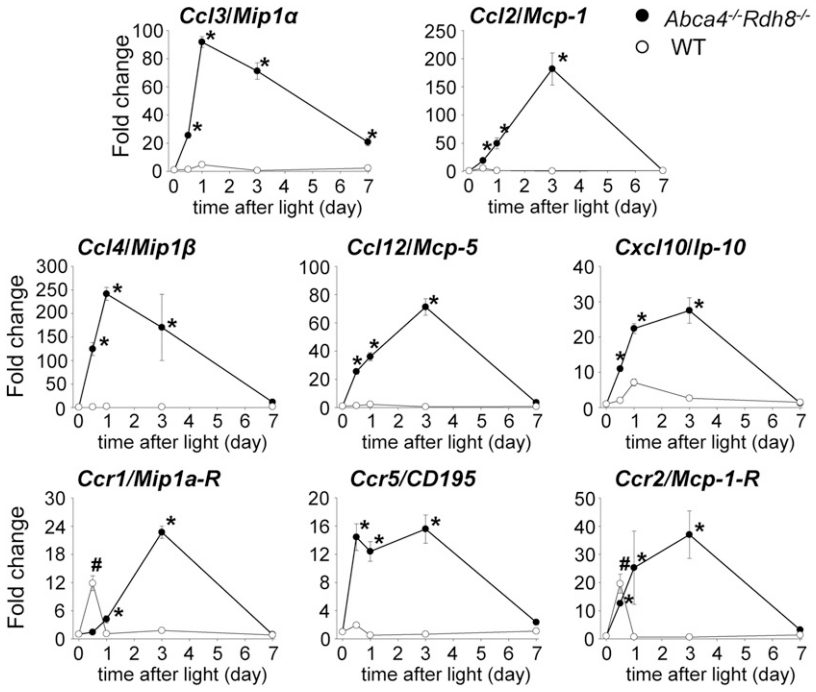

FIGURE 1. Distinct profiles in expression of *Ccl3* and *Ccl2* in the retina of *Abca4*$^{-/-}$*Rdh8*$^{-/-}$ mice after light exposure. Quantitative RT-PCR was performed with RNA purified from 16 retinas of 4-wk-old *Abca4*$^{-/-}$*Rdh8*$^{-/-}$ and WT mice at each time point. Fold changes in expression to unexposed *Abca4*$^{-/-}$*Rdh8*$^{-/-}$ or WT mice are presented. The expression of each gene was normalized to the housekeeping gene *Gapdh*. Error bars indicate SD of the means (n = 3). $^{*}p < 0.05$ versus unexposed *Abca4*$^{-/-}$*Rdh8*$^{-/-}$ mice, $^{\#}p < 0.05$ versus no light exposed WT mice.

Ccl3 and Ccl2 from these cells were measured by ELISA. Only primary microglia revealed an increase in Ccl3 secretion (Supplemental Fig. 1), whereas both primary RPE and microglial cells increased their Ccl2 secretion, indicating that microglia and monocytes are the dominant cells producing Ccl3 rather than RPE.

Low-grade chronic inflammation in retinas of Abca4$^{-/-}$*Rdh8*$^{-/-}$ *mice*

Given the different gene expression patterns of these factors in the retina, we sought to determine whether they have distinct roles in acute versus chronic retinal degeneration in *Abca4*$^{-/-}$*Rdh8*$^{-/-}$ mice (16). Expression levels of the chemokine and chemokine receptor transcripts were examined in 4-wk-, 6-mo- and 12-mo-old *Abca4*$^{-/-}$*Rdh8*$^{-/-}$ and WT mice to assess the changes associated with chronic degeneration of the retina under room light conditions (Fig. 2). Compared with 4-wk-old mice, expression of MIP-1–related genes, including *Ccl3*, *Ccl4*, and *Ccr1*, was increased at the mRNA level in 6-mo-old and decreased in 12-mo-old *Abca4*$^{-/-}$*Rdh8*$^{-/-}$ mice, although *Ccr5,* which is also a receptor of *Ccl3* and *Ccl4*, was increased until 12 mo old. In contrast, MCP-related genes, including *Ccl2* and *Ccl12*, were increased at 12 mo of age. *Ccr2*, a receptor of the *Ccl2* ligand, was also increased at age of 6 and 12 mo. *Cxcl10* displayed a similar expression pattern as MIP-1 genes. These data indicate the presence of low-grade chronic inflammation in the retina of aged *Abca4*$^{-/-}$*Rdh8*$^{-/-}$ mice as observed in human degenerative retinal diseases (1).

Delayed clearance of subretinal microglia in Ccl3$^{-/-}$*Abca4*$^{-/-}$*Rdh8*$^{-/-}$ *mice compared with Abca4*$^{-/-}$*Rdh8*$^{-/-}$ *mice*

Because of the distinct expression pattern of MIP-1 genes, *Ccl3* and *Ccl4*, and other chemokines, we hypothesized that MIP-1 gene products have a distinct role in all-*trans*-retinal mediated retinal degeneration. To assess this hypothesis directly, *Ccl3*$^{-/-}$*Abca4*$^{-/-}$*Rdh8*$^{-/-}$ mice were generated by crossing *Abca4*$^{-/-}$*Rdh8*$^{-/-}$ with *Ccl3*$^{-/-}$ mice. Littermate controls were also generated from this mouse cross. To examine the role of CCL3 in acute retinal degeneration, *Ccl3*$^{-/-}$*Abca4*$^{-/-}$*Rdh8*$^{-/-}$, *Abca4*$^{-/-}$*Rdh8*$^{-/-}$, and WT mice were exposed to 10,000 lx light for 30 min. This light exposure caused more autofluorescent (AF) spots, which was detected by in vivo SLO, which provides a high-quality images by acquiring florescent signals of the retina with a horizontal–confocal view (21) (Fig. 3A). We found significantly more AF spots in *Ccl3*$^{-/-}$*Abca4*$^{-/-}$*Rdh8*$^{-/-}$ mice when compared with *Abca4*$^{-/-}$*Rdh8*$^{-/-}$ mice 14 and 21 d after light exposure. In comparison, *Ccl3*$^{-/-}$ mice did not develop retinal degeneration by the same light exposure condition as *Abca4*$^{-/-}$*Rdh8*$^{-/-}$ mice, and displayed similar resistance to light induced damage as WT mice (Supplemental Fig. 2).

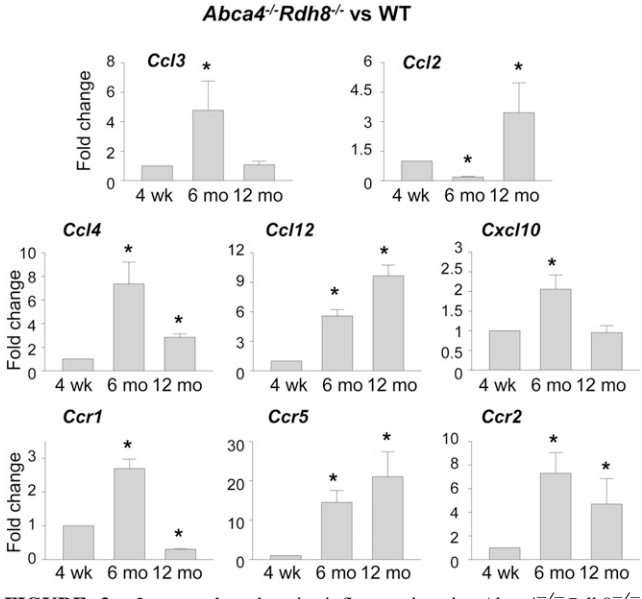

FIGURE 2. Low-grade, chronic inflammation in *Abca4*$^{-/-}$*Rdh8*$^{-/-}$ mice. Quantitative RT-PCR was performed with RNA purified from 16 retinas of 4-wk-old, 6-mo-old, and 12-mo-old *Abca4*$^{-/-}$*Rdh8*$^{-/-}$ and WT mice. The expression of genes in *Abca4*$^{-/-}$*Rdh8*$^{-/-}$ mice was compared with WT mice after normalization to the housekeeping gene *Gapdh*, and presented by fold changes. Error bars indicate SD of the means (n = 3). $^{*}p < 0.05$ versus 4-wk-old mice.

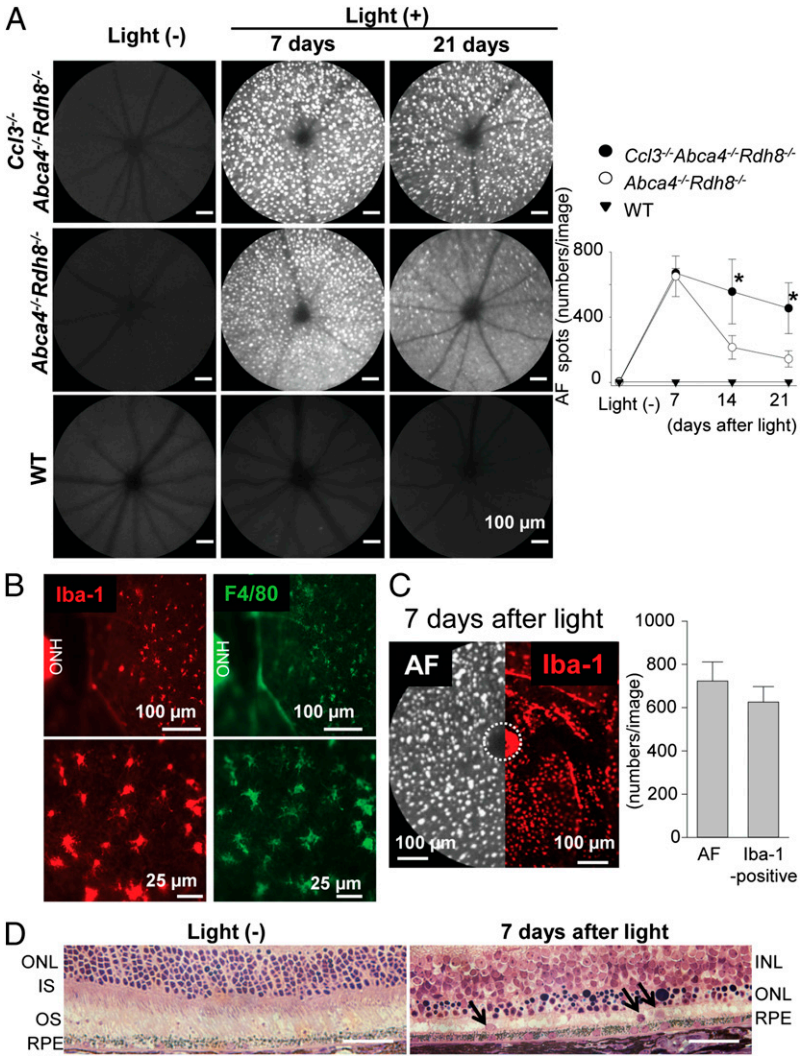

FIGURE 3. Extended appearance of microglia/macrophage in the subretinal space in *Ccl3*$^{-/-}$*Abca4*$^{-/-}$*Rdh8*$^{-/-}$ mice after light exposure. *Ccl3*$^{-/-}$*Abca4*$^{-/-}$*Rdh8*$^{-/-}$, *Abca4*$^{-/-}$*Rdh8*$^{-/-}$, and WT mice at 4–6 wk old were exposed to 10,000 lx light for 30 min. (**A**) Retinal images were captured by in vivo SLO. Images were taken at 7, 14, and 21 d after light exposure (*left*). Scale bars, 100 μm. Numbers of autofluorescent (AF) spots of each image were counted (*right*). Error bars indicate SD of the means ($n > 6$).*$p < 0.05$ versus light-exposed *Abca4*$^{-/-}$*Rdh8*$^{-/-}$ mice. (**B**) RPE flat-mounts of *Abca4*$^{-/-}$*Rdh8*$^{-/-}$ mice were prepared 7 d after light exposure and stained with anti–Iba-1 (*left*) and anti-F4/80 (*right*) Abs. *Lower panels* show magnified images. (**C**) SLO image (*left*) and flat-mount IHC with anti-Iba-1 Ab (*right*) in the same magnification is presented. *Abca4*$^{-/-}$*Rdh8*$^{-/-}$ mice were exposed to 10,000 lx for 30 min and kept in the dark for 7 d. Numbers of AF spots in SLO images (per image) and Iba-1^{+} cells in IHC in the same size area were counted (*right graph*). ONH is circled by broken line. (**D**) Retinal cross section of *Abca4*$^{-/-}$*Rdh8*$^{-/-}$ mice without light exposure and 7 d after light exposure at 10,000 lx for 30 min was prepared by Epon-embedment. Arrows indicate cells in the subretinal space. Scale bars, 50 μm. INL, inner nuclear layer; IS, inner segment; ONH, optic nerve head; ONL, outer nuclear layer; OS, outer segment.

Flat-mount retinas from these mice 7 d after light exposure displayed many infiltrated cells into the subretinal space. These infiltrated cells stained positive for both Iba-1 (a marker for microglia/macrophage) and F4/80 (a marker for macrophage; Fig. 3B). Immunohistochemical analysis with anti–Iba-1, anti-NIMP-R14 (for neutrophil) and anti-CD3 (for T cell) Abs revealed that most of the subretinal cells were Iba-1–positve cells (Table II, Supplemental Fig. 3). A comparison of an SLO image and a flat-mount image with Iba-1 Ab staining is presented in Fig. 3C. The number of AF spots obtained using SLO and counting Iba-1^{+} cells in flat-mount retinas gave similar results. Retinal histology revealed loss of photoreceptor layers and nuclei of what appear to be infiltrating cells in the subretinal space in *Abca4*$^{-/-}$*Rdh8*$^{-/-}$ mice 7 d after light exposure (Fig. 3D).

As a second approach, we generated *Abca4*$^{-/-}$*Rdh8*$^{-/-}$ mice crossed with *Cx3Cr1*$^{gfp/\Delta}$ mice in which their monocytes express GFP (22). Flat-mount eyes after peeled off the neural retina were examined. Light-exposed *Abca4*$^{-/-}$*Rdh8*$^{-/-}$ mice did not show

Table II. Populations of subretinal cells 7 and 21 d after light exposure at 10,000 lx for 30 min

Mouse Models	Days after Light	Iba-1^{+} (%)	NIMP-R14^{+} (%)[a]	CD3^{+} (%)	Counted Cells per 8 Slides[b]
Abca4$^{-/-}$*Rdh8*$^{-/-}$	7 d	97.9 ± 0.9	2.1 ± 0.9	0	191.5 ± 13.5
Abca4$^{-/-}$*Rdh8*$^{-/-}$	21 d	90.3 ± 4.2	6.9 ± 1.0	2.4 ± 2.2	59.7 ± 18.6
Ccl3$^{-/-}$*Abca4*$^{-/-}$*Rdh8*$^{-/-}$	7 d	98.6 ± 2.8	1.3 ± 0.5	0	198.2 ± 21.7
Ccl3$^{-/-}$*Abca4*$^{-/-}$*Rdh8*$^{-/-}$	21 d	91.4 ± 6.2	5.4 ± 0.7	2.8 ± 1.5	147.7 ± 24.1
		GFP^{+} (%)			Counted Cells[c]
Cx3Cr1$^{gfp/\Delta}$*Abca4*$^{-/-}$*Rdh8*$^{-/-}$	7 d	100			1034

[a]NIMP-R14 recognizes Ly6C in addition to Ly6G, and can therefore react with activated microglia/macrophages. As shown in Supplemental Fig. 3, subretinal cells with stronger signals over background or weakly stained cells were counted as positive cells.

[b]Cryosections were prepared from every 200 μm distance from the edge to edge (eight slides per eye), and IHC was performed with anti–Iba-1 Ab for microglia/macrophage, anti–Nimp-R14 Ab for neutrophil and anti-CD3 Ab for T cell. Numbers of subretinal cells were counted from these sections, and the ratio of these cells was calculated.

[c]Flat-mount eyes were prepared and subretinal cells with GFP, and autofluorescent signals were counted under fluorescent microscope.

GFP$^+$ cells on the apical side of RPE layer, whereas *Cx3Cr1*$^{gfp/\Delta}$ *Abca4*$^{-/-}$*Rdh8*$^{-/-}$ mice after induction of retinal light damage demonstrated GFP$^+$ cells above the RPE layers (Fig. 4A). GFP$^+$ cells were not detected before light exposure in either *Cx3Cr1*$^{gfp/\Delta}$ *Abca4*$^{-/-}$*Rdh8*$^{-/-}$ or in *Abca4*$^{-/-}$*Rdh8*$^{-/-}$ mice, indicating translocation of microglial/macrophage cells from the inner retina to the subretinal space. Ramified shaped GFP$^+$ cells were observed only in the inner retina prior to light exposure, and no GFP$^+$ cells were detected in the subretinal space (Fig. 4B, *upper panel*). In contrast, eyes of *Cx3Cr1*$^{gfp/\Delta}$*Abca4*$^{-/-}$*Rdh8*$^{-/-}$ mice 7 d after light exposure displayed increased numbers of more rounded GFP$^+$ cells in the deeper retina close to the RPE layer (Fig. 4B, *lower panel*). Multiple GFP$^+$ cells were observed in the outer nuclear layers (ONL) as well (Fig. 4C) and GFP$^+$ cells were detected in the subretinal layers (Table II). SLO images of *Cx3Cr1*$^{gfp/\Delta}$*Abca4*$^{-/-}$*Rdh8*$^{-/-}$ mice with and without light exposure showed GFP signals from the inner plexiform layer where resting microglial cells normally reside (Fig. 4D, *upper panel*). Although there were no GFP signals from the level of the subretinal space (OS ~ RPE) before light exposure, GFP and AF signals were detected in the subretinal space of *Cx3Cr1*$^{gfp/\Delta}$ *Abca4*$^{-/-}$*Rdh8*$^{-/-}$ mice following light exposure (Fig. 4D, *lower panel*). As the number of AF spots in light exposed *Abca4*$^{-/-}$ *Rdh8*$^{-/-}$ mice is similar to that of GFP$^+$ cells in *Cx3Cr1*$^{gfp/\Delta}$ *Abca4*$^{-/-}$*Rdh8*$^{-/-}$ mice, it is likely that the AF spots detected with SLO are consistent with microglial cells. RPE flat-mounts from light exposed *Ccl3*$^{-/-}$*Abca4*$^{-/-}$*Rdh8*$^{-/-}$ mice displayed enlarged RPE cells and reduced expression of tight junction protein, Zo-1, compared with light exposed and no light exposed *Abca4*$^{-/-}$*Rdh8*$^{-/-}$ mice, thus indicating a loss of RPE cell integrity and viability (Supplemental Fig. 4). Taken together, these data indicate delayed clearance of microglia and loss of RPE cell integrity in the absence of Ccl3.

Increased expression of chemokines and the other inflammatory molecules in Ccl3$^{-/-}$*Abca4*$^{-/-}$*Rdh8*$^{-/-}$ *mice after light exposure*

Light exposed *Ccl3*$^{-/-}$*Abca4*$^{-/-}$*Rdh8*$^{-/-}$ and *Abca4*$^{-/-}$*Rdh8*$^{-/-}$ mice displayed severe retinal degeneration, although there was a different clearance rate of subretinal infiltrating cells between the two above mentioned mouse lines (Fig. 5A). To elucidate the molecular changes causing the delay in clearance of subretinal microglia/macrophages in *Ccl3*$^{-/-}$*Abca4*$^{-/-}$*Rdh8*$^{-/-}$ mice, mRNA levels of chemokines and other inflammatory molecules in the retina were examined. Although *Ccl3* was completely diminished, *Ccl4*, which has a sequence homology of ~60% with the murine *Ccl3* gene, was increased in *Ccl3*$^{-/-}$*Abca4*$^{-/-}$*Rdh8*$^{-/-}$ mice compared with *Abca4*$^{-/-}$*Rdh8*$^{-/-}$ mice at 3 d and 7 d after light exposure (Fig. 5B). Absolute expression levels of *Ccl3*, *Ccl4*, *Ccl2*, and *Il1b* against the house keeping *Gapdh* gene at 7 d after light are also shown (Fig. 5C). Inflammatory molecules, excluding *Ccl3*, were increased in *Ccl3*$^{-/-}$*Abca4*$^{-/-}$*Rdh8*$^{-/-}$ mice

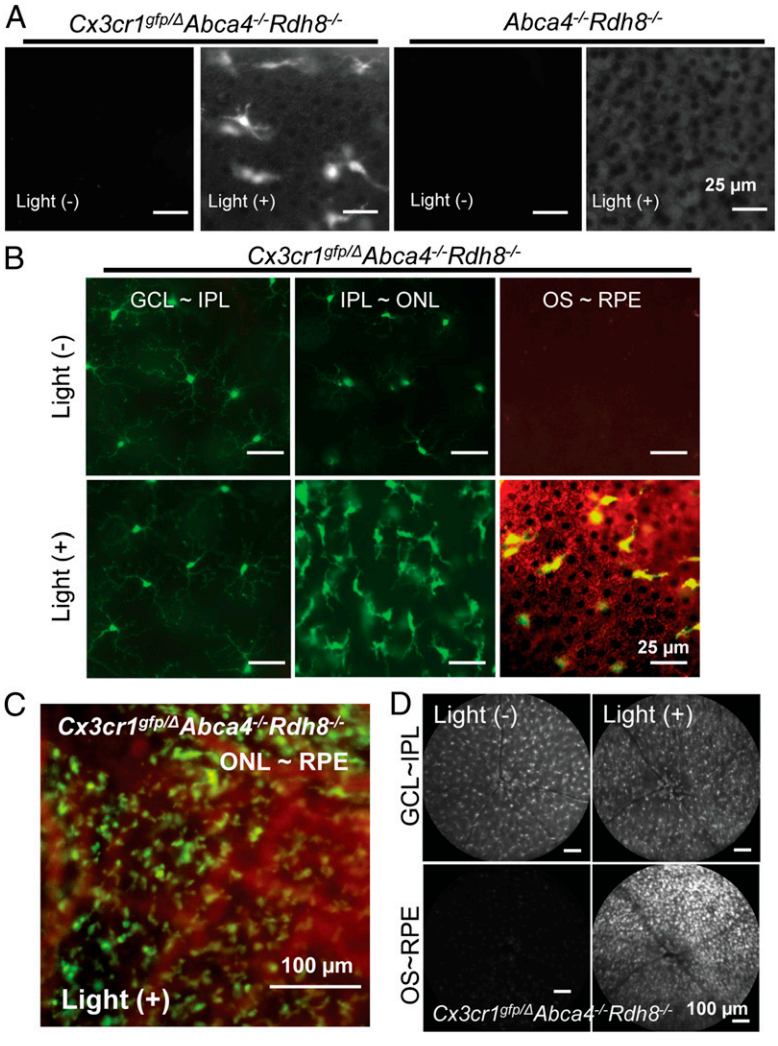

FIGURE 4. Translocation of monocytes during light-induced retinal degeneration. (**A**) Flat-mount RPE was examined 7 d after light exposure at 10,000 lx for 30 min under a fluorescent microscope with 4-wk-old *Cx3Cr1*$^{gfp/\Delta}$ *Abca4*$^{-/-}$*Rdh8*$^{-/-}$ and *Abca4*$^{-/-}$*Rdh8*$^{-/-}$ mice. Scale bars, 25 μm. (**B**) Shapes of GFP$^+$ cells were examined in 4-wk-old *Cx3Cr1*$^{gfp/\Delta}$*Abca4*$^{-/-}$*Rdh8*$^{-/-}$ mice by flat-mount eyes 7 d after exposure to light at 10,000 lx for 30 min at different depth of the retina. GFP signals are shown in green in the left and right panels and autofluorescent signals are shown in red. Scale bars, 25 μm. (**C**) GFP$^+$ cells at the ONL ~ RPE level is presented. *Cx3Cr1*$^{gfp/\Delta}$ *Abca4*$^{-/-}$*Rdh8*$^{-/-}$ mice were exposure to light at 10,000 lx for 30 min and flat-mount retina was prepared 7 d after light. Scale bar, 100 μm. (**D**) SLO images were captured from 4-wk-old *Cx3Cr1*$^{gfp/\Delta}$*Abca4*$^{-/-}$*Rdh8*$^{-/-}$ mice before and 7 d after light exposure at 10,000 lx for 30 min. Scale bars, 100 μm. GCL, ganglion cell layer; IPL, inner plexiform layer; ONL, outer nuclear layer; RPE, retinal pigment epithelium.

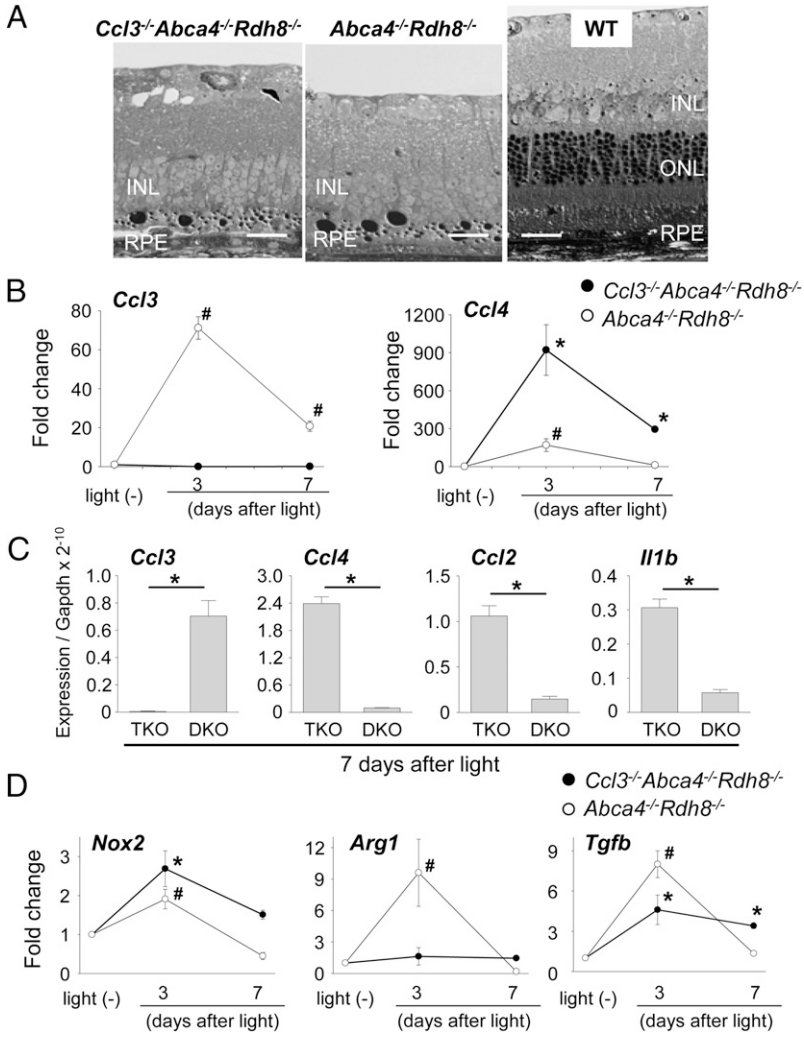

FIGURE 5. Elevated mRNA expressions of inflammatory molecules in the retinas of light exposed $Ccl3^{-/-}Abca4^{-/-}Rdh8^{-/-}$ mice. (**A**) Severity of retinal degeneration in 4-wk-old $Ccl3^{-/-}Abca4^{-/-}Rdh8^{-/-}$, $Abca4^{-/-}Rdh8^{-/-}$, and WT mice after light exposure at 10,000 lx for 30 min was examined by epon-embedment sections 7 d after light exposure. Scale bars, 30 μm. (**B**) RNA samples were collected from 16 retinas of 4-wk-old $Ccl3^{-/-}Abca4^{-/-}Rdh8^{-/-}$ (TKO) and $Abca4^{-/-}Rdh8^{-/-}$ (DKO) at each point. *Ccl3* and *Ccl4* mRNA expression levels were examined by quantitative RT-PCR. Data are normalized by *Gapdh* expression and shown by fold change. Error bars indicate SD of the means ($n = 3$). $^{\#}p < 0.05$ versus no light exposed $Abca4^{-/-}Rdh8^{-/-}$ mice. (**C**) Absolute expression levels of *Ccl3*, *Ccl4*, *Ccl2*, and *Il1b* mRNA at 7 d after light were shown when compared with *Gapdh* expression. Error bars indicate SD of the means ($n = 3$). $^{*}p < 0.05$ between each group. (**D**) RNA samples were collected from 16 retinas of mice at each point. Expression levels of *Nox2*, a marker of M1 microglia/macrophage, *Arg1*, a marker of M2 microglia/macrophage, and *Tgfb* are normalized by *Gapdh* expression and shown by fold change. Error bars indicate SD of the means ($n = 3$). $^{*}p < 0.05$ versus no light exposed $Ccl3^{-/-}Abca4^{-/-}Rdh8^{-/-}$ mice, $^{\#}p < 0.05$ versus no light exposed $Abca4^{-/-}Rdh8^{-/-}$ mice. INL, inner nuclear layer; ONL, outer nuclear layer; RPE, retinal pigment epithelium.

compared with $Abca4^{-/-}Rdh8^{-/-}$ mice. Expression of M1 and M2 microglia/macrophage related molecules were also evaluated (Fig. 5D), because M1 macrophages contribute to inflammation, whereas M2 macrophages have an anti-inflammatory role (23). *Nox2*, a prototypic M1 microglia/macrophage marker (24) was increased in both $Ccl3^{-/-}Abca4^{-/-}Rdh8^{-/-}$ and $Abca4^{-/-}Rdh8^{-/-}$ mice at 3 d after light exposure. However, expression of *Arg1*, a marker of M2 microglia/macrophage (17), was increased only in $Abca4^{-/-}Rdh8^{-/-}$ mice 3 d after light. *Tgfb*, an immunosuppressive factor and component of the immune-privilege in the eye (25), was elevated in $Abca4^{-/-}Rdh8^{-/-}$ mice at 3 d, but returned to basal levels 7 d after light exposure.

Severe retinal degeneration develops in $Ccl3^{-/-}Abca4^{-/-}Rdh8^{-/-}$ mice after brief light exposure

Because $Ccl3^{-/-}Abca4^{-/-}Rdh8^{-/-}$ and $Abca4^{-/-}Rdh8^{-/-}$ mice both exhibited similar levels of retinal degeneration after 30 min of light exposure at 10,000 lx, it is unclear what effect *Ccl3* has on light-induced photoreceptor cell death. However, because $Ccl3^{-/-}Abca4^{-/-}Rdh8^{-/-}$ mice showed prolonged retinal inflammation after light exposure, we examined the effect of Ccl3 on mice exposed to 10,000 lx light for 15 min, which is only half the duration of our usual light exposure period. $Ccl3^{-/-}Abca4^{-/-}Rdh8^{-/-}$ mice exhibited severe retinal degeneration compared with $Abca4^{-/-}Rdh8^{-/-}$ mice 7 d after light exposure (Fig. 6A). Furthermore, $Ccl3^{-/-}Abca4^{-/-}Rdh8^{-/-}$ mice exposed to 15 min of light showed higher Iba-1^{+} cell accumulation in the subretinal space and increased numbers of AF spots compared with $Abca4^{-/-}Rdh8^{-/-}$ mice (Fig. 6B, 6C). Additional production of Ccl3 after light exposure at 10,000 lx for 15 min was observed in $Abca4^{-/-}Rdh8^{-/-}$ mice, whereas Ccl3 production was not detected in $Ccl3^{-/-}Abca4^{-/-}Rdh8^{-/-}$ mice by ELISA (Fig. 6D). Furthermore, elevated production of Ccl4 was documented in $Ccl3^{-/-}Abca4^{-/-}Rdh8^{-/-}$ mice compared with $Abca4^{-/-}Rdh8^{-/-}$ mice 1 and 3 d after light exposure. Increased production of Il-1β (130.8 ± 53.5 pmol/eye in $Ccl3^{-/-}Abca4^{-/-}Rdh8^{-/-}$ mice versus 46.2 ± 8.8 pmol/eye in $Abca4^{-/-}Rdh8^{-/-}$ mice) was also detected 1 d after light exposure in $Ccl3^{-/-}Abca4^{-/-}Rdh8^{-/-}$ mice. Taken together, these data indicate that *Ccl3* deficiency exacerbates acute light-induced retinal degeneration with more production of Ccl4 in $Abca4^{-/-}Rdh8^{-/-}$ mice.

Ccl3 deficiency moderates age-related retinal degeneration in $Abca4^{-/-}Rdh8^{-/-}$ mice

Our previous studies showed that age-related retinal degeneration in $Abca4^{-/-}Rdh8^{-/-}$ mice is characterized by chronic and sustained low-grade retinal inflammation (2, 16). To elucidate the role of CCL3 in chronic degeneration compared with light induced acute degeneration, the retinal phenotype of 6-mo-old $Ccl3^{-/-}Abca4^{-/-}Rdh8^{-/-}$ and $Abca4^{-/-}Rdh8^{-/-}$ mice were examined. We found severe retinal degeneration in $Abca4^{-/-}Rdh8^{-/-}$ mice compared with WT mice by SD-OCT, which displays a tangential

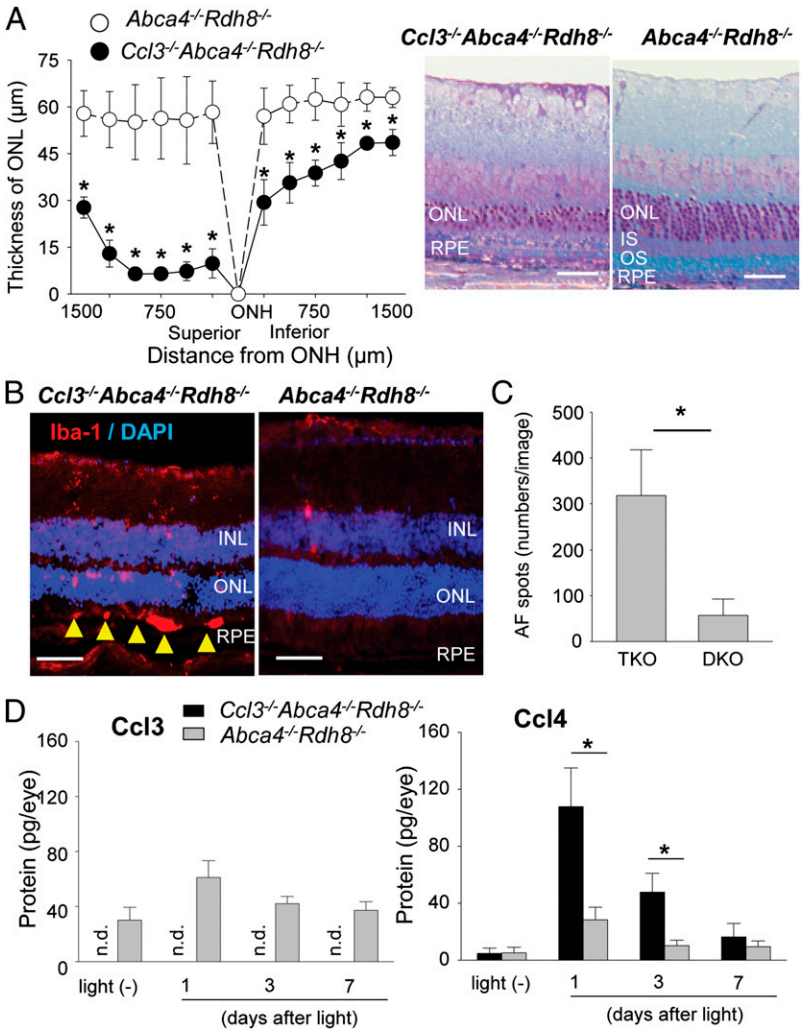

FIGURE 6. More severe retinal degeneration in *Ccl3*$^{-/-}$*Abca4*$^{-/-}$*Rdh8*$^{-/-}$ mice than in *Abca4*$^{-/-}$*Rdh8*$^{-/-}$ mice after 15 min of light exposure. Four 6-wk-old *Ccl3*$^{-/-}$*Abca4*$^{-/-}$*Rdh8*$^{-/-}$ (TKO) and *Abca4*$^{-/-}$*Rdh8*$^{-/-}$ (DKO) mice were exposed to 10,000 lx light for 15 min. (**A**) Thickness of ONL was measured by SD-OCT (*left*) and retinal sections (*right*) were prepared at 7 d after light exposure. Error bars indicate SD of the means ($n > 6$). *$p < 0.05$ versus light exposed *Abca4*$^{-/-}$*Rdh8*$^{-/-}$ mice. Scale bars, 50 μm. (**B**) IHC by using anti–Iba-1, a marker of microglia/macrophage, 7 d after light exposure for 15 min are presented. Yellow arrowheads indicate infiltrated microglia/macrophages in the subretinal space. Scale bars, 30 μm. (**C**) Numbers of AF spots were counted by using SLO. Error bars indicate SD of the means ($n > 6$). *$p < 0.05$. (**D**) Production of Ccl3 and Ccl4 was quantified by ELISA with eyes before and 1, 3, and 7 d after light exposure at 10,000 lx for 15 min. Two eyes from one mouse were homogenized in 500 μl of PBS with proteinase inhibitors, and the homogenates (50 μl) were used for the quantification. Error bars indicate SD of the means ($n > 3$ mice). *$p < 0.05$. INL, inner nuclear layer; IS, inner segments; n.d., not detectable; ONL, outer nuclear layer; OS, outer segments; RPE, retinal pigment epithelium.

view of the retina with ultrahigh resolution in vivo (26). Retinal degeneration in 6-mo-old *Ccl3*$^{-/-}$*Abca4*$^{-/-}$*Rdh8*$^{-/-}$ mice resembled WT mice (Fig. 7A, 7B), indicating reversal of the *Abca4*$^{-/-}$*Rdh8*$^{-/-}$ phenotype in the absence of Ccl3. GFAP expression was also weaker in 6-mo-old *Ccl3*$^{-/-}$*Abca4*$^{-/-}$*Rdh8*$^{-/-}$ mice than in *Abca4*$^{-/-}$*Rdh8*$^{-/-}$ mice (Fig. 7A, *lower panel*), indicating milder reactive gliosis against retinal inflammation. Furthermore, the number of AF spots, which represent subretinal microglial/macrophage cells (2), was also decreased in 6-mo-old *Ccl3*$^{-/-}$*Abca4*$^{-/-}$*Rdh8*$^{-/-}$ mice (Fig. 7C). Production of Ccl3, Ccl4 and Il-1β was quantified with the eyes of 6-mo-old mice by ELISA (Fig. 7D). *Ccl3*$^{-/-}$*Abca4*$^{-/-}$*Rdh8*$^{-/-}$ mice showed no production of Ccl3, but 139.1 ± 41.1 pg/eye of Ccl3 was detected in *Abca4*$^{-/-}$*Rdh8*$^{-/-}$ mice. Basal Ccl3 production was observed in WT mice between mice at 6 mo of age (36.8 ± 0.93 pg/eye) and 6 wk of age (37.3 ± 6.3 pg/eye). Decreased production of Ccl4 and Il-1β was noted in *Ccl3*$^{-/-}$*Abca4*$^{-/-}$*Rdh8*$^{-/-}$ retinas compared with *Abca4*$^{-/-}$*Rdh8*$^{-/-}$ retinas. Collectively, these findings indicate that Ccl3 enhances age-related retinal degeneration and inflammation in *Abca4*$^{-/-}$*Rdh8*$^{-/-}$ mice, which is the opposite effect that Ccl3 has on acute retinal degeneration caused by light.

Ccl3 deficiency results in increased photoreceptor survival in a murine model of retinitis pigmentosa

The role of CCL3 in retinal degeneration was further examined in the *Mertk*$^{-/-}$ mouse model of retinitis pigmentosa. Mutations in the *MERTK* gene cause retinal dystrophies in humans and in animal models (27). MERTK belongs to a family of receptor tyrosine kinases that includes AXL and TYRO3, and it plays an indispensable role in the clearance of photoreceptor debris by RPE phagocytosis (28). Accumulation of photoreceptor debris in the subretinal space because of RPE phagocytosis deficiency is closely associated with the photoreceptor cell death seen in the Royal College of Surgeons rat with disabled Mertk and in *Mertk*$^{-/-}$ mice (29). To determine whether the retinal degenerative phenotype of *Mertk*$^{-/-}$ mice was altered in the absence of Ccl3, *Ccl3*$^{-/-}$*Mertk*$^{-/-}$ mice were generated, and the thickness of ONL in *Ccl3*$^{-/-}$*Mertk*$^{-/-}$, *Mertk*$^{-/-}$ and WT mice was assessed at 5 and 8 wk of age by in vivo SD-OCT imaging. *Mertk*$^{-/-}$ mice showed degraded ONL compared with WT mice; however, *Ccl3*$^{-/-}$*Mertk*$^{-/-}$ mice had increased ONL thickness when compared with *Mertk*$^{-/-}$ mice, but was still less than WT mice (Fig. 8A). Representative retinal histology images of 5-wk-old *Ccl3*$^{-/-}$*Mertk*$^{-/-}$, *Mertk*$^{-/-}$, and WT mice are shown (Fig. 8B). Fewer numbers of Iba-1^{+} cells were noted in *Ccl3*$^{-/-}$*Mertk*$^{-/-}$ mice than in *Mertk*$^{-/-}$ mice at 5 and 8 wk of age (Fig. 8C). Because inflammation in damaged retinas affects the integrity of the inner blood-retinal barrier (2), the integrity of this barrier in 8-wk-old *Ccl3*$^{-/-}$*Mertk*$^{-/-}$, *Mertk*$^{-/-}$, and WT mice was examined by fluorescent angiography. Whereas *Ccl3*$^{-/-}$*Mertk*$^{-/-}$ mice showed only weak fluorescent dye leakage from the optic nerve head (ONH), *Mertk*$^{-/-}$ mice showed increased leakage not only from ONH but also from retinal

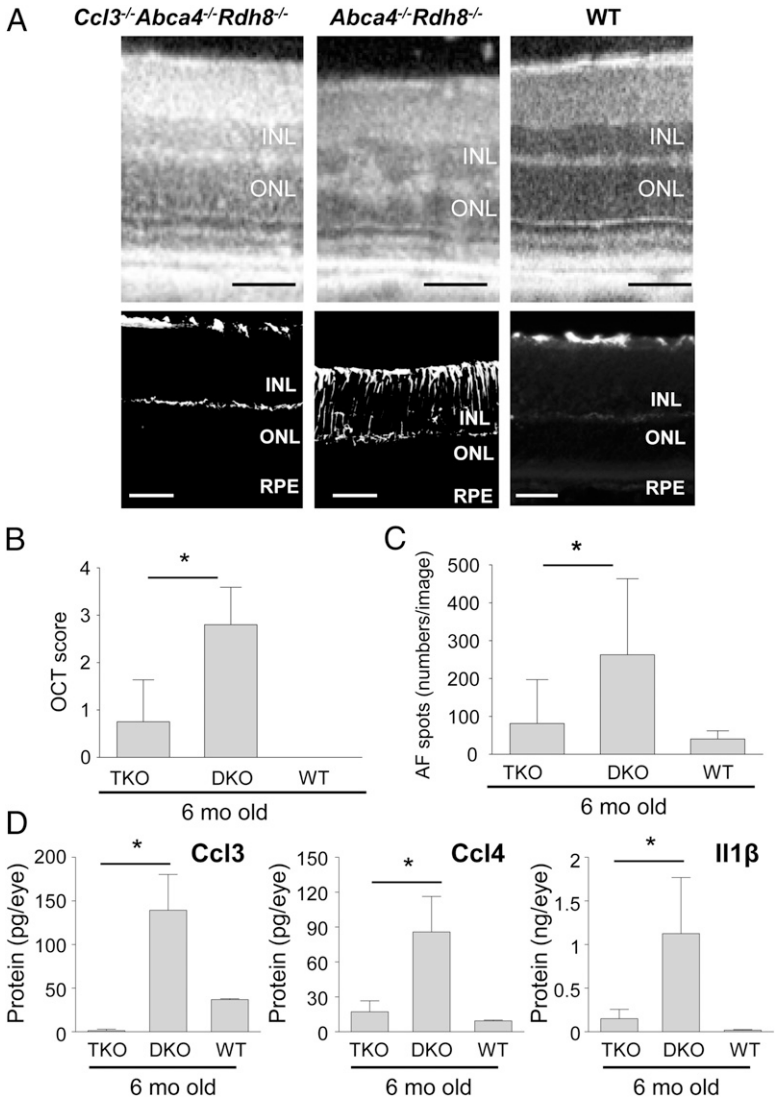

FIGURE 7. *Ccl3* deficiency attenuated age-related retinal degeneration in $Abca4^{-/-}Rdh8^{-/-}$ mice. (**A**) Retinal phenotype of $Ccl3^{-/-}Abca4^{-/-}Rdh8^{-/-}$ (TKO) and $Abca4^{-/-}Rdh8^{-/-}$ (DKO) mice at 6 mo old were examined by in vivo SD-OCT imaging (*upper panels*), and IHC staining by GFAP, a marker for Müller cell gliosis (*lower panels*). Scale bars, 50 μm. (**B**) Severity of retinal degeneration was evaluated with an established scoring system (20). (**C**) Numbers of AF spots at 6 mo of age were counted. Error bars indicate SD of the means ($n > 5$). (**D**) Production of Ccl3, Ccl4, and Il-1β was quantified by ELISA. Two eyes of 6-mo-old mice were homogenized in 500 μl PBS with proteinase inhibitors, and the homogenates (50 μl) were used for the quantification. Error bars indicate SD of the means ($n > 3$ mice). $*p < 0.05$. INL, inner nuclear layer; ONL, outer nuclear layer; RPE, retinal pigment epithelium.

vessels (Fig. 8D). The incidence of fluorescent dye leakage in $Ccl3^{-/-}Mertk^{-/-}$, $Mertk^{-/-}$, and WT mice from the ONH were 33.3%, 83.3%, and 0%, respectively. These findings indicate that the deficiency of Ccl3 contributed to milder retinal degeneration in the $Mertk^{-/-}$ mouse model of retinitis pigmentosa.

Ccl2 deficiency protects the retina from degeneration in mouse models

To elucidate the role of CCL3 and CCL2 further in the pathophysiology of retinal degeneration, $Ccl2^{-/-}Abca4^{-/-}Rdh8^{-/-}$ mice were generated by crossing $Abca4^{-/-}Rdh8^{-/-}$ with $Ccl2^{-/-}$ mice. $Ccl2^{-/-}Mertk^{-/-}$ mice were also generated. After light exposure at 10,000 lx for 30 min, $Ccl2^{-/-}Abca4^{-/-}Rdh8^{-/-}$ mice showed better preservation of the ONL (Fig. 9A, *left panel*) and fewer AF spots/Iba-1$^+$ cells in the subretinal space (Fig. 9A, *right panel*) compared with $Abca4^{-/-}Rdh8^{-/-}$ mice. Less severe age-related retinal degeneration with fewer AF spots was also observed in $Ccl2^{-/-}Abca4^{-/-}Rdh8^{-/-}$ mice compared with $Abca4^{-/-}Rdh8^{-/-}$ mice at 6 mo of age (Fig. 9B). In addition, $Ccl2^{-/-}Mertk^{-/-}$ mice revealed a more intact ONL when compared with $Mertk^{-/-}$ mice at 5 and 8 wk of age (Fig. 9C). Therefore, loss of Ccl2 resulted in milder retinal degeneration in all three models of retinal degeneration.

Discussion

Our previous studies with the retinal degeneration model of $Abca4^{-/-}Rdh8^{-/-}$ mice implicated a role for RPE-derived chemokines and cytokines in recruitment of tissue microglia from the inner retina to the subretinal space (2). Although the increased number of Iba-1 cells is likely due to infiltration, we cannot exclude the possibility that an increase in Iba-1$^+$ cells is not due to cell proliferation. Retinal vascular endothelial cells are also a potential source of these chemokines in vivo, especially in recruitment of monocytes into the inner retina. In the current study, transcript level analysis of chemokines in the retina of $Abca4^{-/-}Rdh8^{-/-}$ mice revealed selective elevation of Ccl3 and Ccl4 24 h after light exposure among tested chemokines. WT mice did not develop light-induced retinal degeneration and increased production of Ccl3 and Ccl4 was not documented. Furthermore, although most chemokines have overlapping targets in terms of receptor binding, by generating $Ccl3^{-/-}Abca4^{-/-}Rdh8^{-/-}$ mice, we demonstrated a nonredundant role for CCL3 in retinal degeneration.

CCL3 is likely produced by subretinally translocated tissue microglia from the inner retina where they normally reside, and this can be a trigger for additional monocyte infiltration from the circulation via inner retinal blood vessels. Prolonged activation of resident microglia is also observed in experimental herpes en-

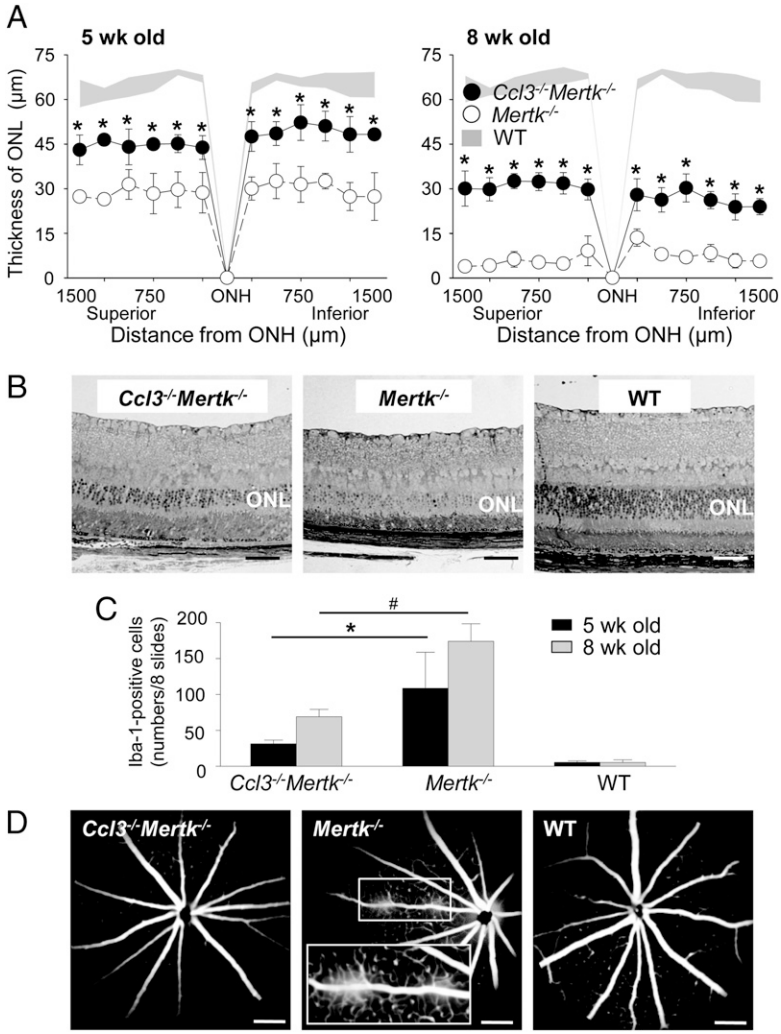

FIGURE 8. *Ccl3* deficiency protects the retina from degeneration in the mouse model for retinitis pigmentosa. $Ccl3^{-/-}Mertk^{-/-}$ mice were established by crossing between $Mertk^{-/-}$ and $Ccl3^{-/-}$ mice. Littermate $Mertk^{-/-}$ mice were used as control. (**A**) Thickness of ONL from $Ccl3^{-/-}Mertk^{-/-}$, $Mertk^{-/-}$, and WT mice at 5 and 8 wk of age were measured by SD-OCT. Error bars indicate SD of the means ($n > 6$). $*p < 0.05$ versus $Mertk^{-/-}$ mice. (**B**) Images of retinal histology from 5-wk-old $Ccl3^{-/-}Mertk^{-/-}$, $Mertk^{-/-}$, and WT mice are shown. Scale bars, 50 μm. (**C**) Iba-1^{+} cells in the subretinal space were counted using cryosections from $Ccl3^{-/-}Mertk^{-/-}$, $Mertk^{-/-}$, and WT mice at 5 and 8 wk of age. These cryosections were prepared every 200 μm distance from edge to edge (eight slides per eye), and IHC was performed with anti–Iba-1 Ab. Error bars indicate SD of the means ($n > 6$). $*,^{\#}p < 0.05$. (**D**) Fluorescent angiography from 8-wk-old $Ccl3^{-/-}Mertk^{-/-}$, $Mertk^{-/-}$, and WT mice are presented. Scale bars, 100 μm. Magnified images of solid line inset shown in the broken rectangle. ONL, outer nuclear layer;

cephalitis, experimental autoimmune encephalomyelitis, and myocardial infarction (30–32).

The ingestion of POS by RPE cells is essential for the maintenance of retinal health (33). However, RPE cells can also contribute to retinal inflammation when POS phagocytosis is disrupted or abnormal (1). Our previous study implicated RPE cells as a source of chemokines that contribute to migration of tissue microglia from the inner retina to the subretinal space (2). These microglial cells also ingest photoreceptor debris, and thereby display increased autofluorescence signals and increased production of proinflammatory and chemotactic cytokines. This results in further infiltration of monocytes from the circulation and promotes their migration from capillaries in the inner retina to the subretinal space. Previous studies using GFP-chimeras of myeloid cells had increased accumulation of monocytes in the subretinal space after light induced retinal damage (34). In addition to RPE cells and microglia, other cells produce Ccl3 including astrocytes and Müller cells. Of particular consideration is that light-exposed $Abca4^{-/-}Rdh8^{-/-}$ mice showed reactive gliosis in these cells (2). Their interaction with the vascular endothelium might also be associated with chemokine production as observed in neural inflammation in the CNS (35, 36).

When $Ccl3^{-/-}Abca4^{-/-}Rdh8^{-/-}$ and littermate $Abca4^{-/-}Rdh8^{-/-}$ mice were exposed to 10,000 lx of light for 30 min, light-exposed $Ccl3^{-/-}Abca4^{-/-}Rdh8^{-/-}$ mice showed delayed clearance of infiltrated microglia from the subretinal space compared with $Abca4^{-/-}Rdh8^{-/-}$ mice. Although light-exposed $Ccl3^{-/-}Abca4^{-/-}Rdh8^{-/-}$ mice did not secrete any *Ccl3*, a substantial increase of *Ccl4* was observed in these mice compared with $Abca4^{-/-}Rdh8^{-/-}$ mice after light exposure. Furthermore, $Ccl3^{-/-}Abca4^{-/-}Rdh8^{-/-}$ mice also displayed an increase of *Ccl2* and *Il1b*, which are hallmarks of retinal inflammation after light (1). These observations indicate persistent retinal inflammation, which contributes to the severity of retinal degeneration in light-exposed $Ccl3^{-/-}Abca4^{-/-}Rdh8^{-/-}$ mice.

Results of the current study also show unchanged expression of *Arg1*, a marker of M2 macrophages in $Ccl3^{-/-}Abca4^{-/-}Rdh8^{-/-}$ mice before and after light exposure, whereas changes in expression of the *Nox2* gene, which is a prototypic M1 marker (24), were observed in $Ccl3^{-/-}Abca4^{-/-}Rdh8^{-/-}$ and $Abca4^{-/-}Rdh8^{-/-}$ mice. CCR2-associated M1 monocytes contribute to the digestion of damaged tissue, whereas Cx3Cr1-associated M2 monocytes promote healing in cases of myocardial infarction (30–32). Accumulating evidence in other chronic diseases implies that the lack of Arg1 elevation in light exposed $Ccl3^{-/-}Abca4^{-/-}Rdh8^{-/-}$ mice balances the local environment to inflammatory state and thus contributes to persistent retinal inflammation. We additionally showed data that supports a nonredundant role for CCL3 in a second model of retinal degeneration the $Mertk^{-/-}$ mouse. $Ccl3^{-/-}Mertk^{-/-}$ mice displayed a less severe and less frequent impairment of the blood-retinal-barrier compared with $Mertk^{-/-}$ mice.

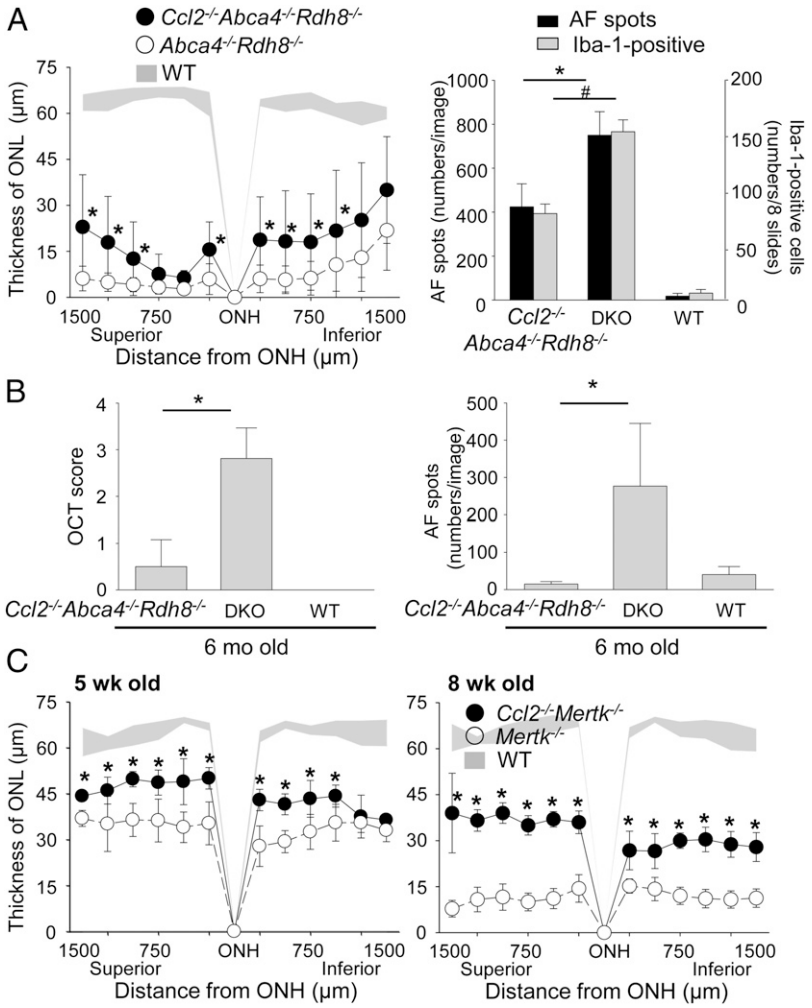

FIGURE 9. *Ccl2* deficiency protects the retina from degeneration in $Abca4^{-/-}Rdh8^{-/-}$ mice and $Mertk^{-/-}$ mice. (**A**) $Ccl2^{-/-}Abca4^{-/-}Rdh8^{-/-}$, $Abca4^{-/-}Rdh8^{-/-}$ (DKO), and WT mice at 4–6-wk-old age were exposed to 10,000 lx light for 30 min. Thickness of ONL was measured by SD-OCT at 7 d after light exposure (*left*). Error bars indicate SD of the means ($n > 6$).*$p < 0.05$ versus light exposed $Abca4^{-/-}Rdh8^{-/-}$ mice. Numbers of AF spots of each image of SLO and Iba-1^+ cells in the subretinal space were counted 7 d after light exposure (*right*). Cryosections were prepared every 200 μm distance from the edge to edge (eight slides per eye), and IHC was performed with anti–Iba-1 Ab. Error bars indicate SD of the means ($n > 6$).*,#$p < 0.05$. (**B**) $Ccl2^{-/-}Abca4^{-/-}Rdh8^{-/-}$, $Abca4^{-/-}Rdh8^{-/-}$ (DKO), and WT were kept under regular light conditions (12h ∼ 10 lx, 12 h dark), and retinal phenotype of these mice were characterized at the age of 6 mo. Severity of retinal degeneration was evaluated with an established scoring system (20) with in vivo OCT imaging (*left*). Numbers of AF spots was counted by in vivo SLO imaging (*right*). *$p < 0.05$. (**C**) Thickness of ONL from $Ccl2^{-/-}Mertk^{-/-}$, $Mertk^{-/-}$, and WT mice at 5 and 8 wk old age were measured by SD-OCT. Error bars indicate SD of the means ($n > 6$). *$p < 0.05$ versus $Mertk^{-/-}$ mice. ONL, outer nuclear layer;

Macrophage/microglia has M1 and M2 subpopulations, which can regulate severity of AMD pathology (37, 38). M1 and M2 cells are also reported to play important roles in other inflammation models for many degenerative diseases (39). Persistent inflammation after traumatic brain injury is known to promote progression to Alzheimer disease (40). The proinflammatory M1 type microglia-based inflammatory mechanism has been shown to be involved in progression of posttraumatic brain injury to Alzheimer disease for over decades.

Studies of the Alzheimer disease model also implicated a role for CCL2-CCR2 interaction in activation of tissue microglial cells (39) and in the pathogenesis of age-related retinal degeneration in $Ccl2^{-/-}$ and $Ccr2^{-/-}$ mice (6, 41, 42). Conversely, CCL2 and CCR2 were found to have a harmful role in chronic oxidative stress-induced or inherited retinal degeneration, as *Cc2* and *Ccr2* gene knockout mice had less severe retinal degeneration (43, 44). In the current study, increased expression of *Ccl2* in light-exposed $Abca4^{-/-}Rdh8^{-/-}$ mice was observed, in addition to decreased retinal degeneration in $Ccl2^{-/-}Abca4^{-/-}Rdh8^{-/-}$ mice and in the $Ccl2^{-/-}Mertk^{-/-}$ mouse were demonstrated. These data indicate that in our models, CCL2-CCR2 activation accelerates inflammation, possibly by recruiting M1 rather than M2 cells, and that preceded CCL3 production could affect CCL2-CCR2 interaction in degenerative conditions. Differential chemokine networks modulate the severity of disease phenotype, and improved understanding in each disease and disease state could largely contribute to future care of retinal diseases.

CCL3 and its receptors, CCR1 and CCR5, are therapeutic targets for treatment of HIV infection, multiple sclerosis, rheumatoid arthritis, diabetes, endometriosis, organ transplant rejection, and multiple myeloma (45). Given the current findings, CCL3, CCR1, and CCR5 are also potential targets for therapeutic intervention in retinal degeneration; however, further study is required to determine the role of this chemokine at each disease stage. Considering these results, a direct inhibition of microglial cells using drugs for antimicroglial activation, such as minocycline (46), might be beneficial to treat inflammation in degenerative retinal diseases.

In conclusion, this study revealed that production of chemokines was closely associated with degenerative retinal changes and microglia/macrophage translocation into the subretinal space. Regulatory mechanism of chemokine networks were differed in models of retinal degeneration. CCL3 showed a distinct role in pathogenesis of retinal degeneration under acute and chronic conditions in mouse models. Although a preceding increase in CCL3 from retinal microglial cells suggests the role of CCL3 as a potential master regulator of retinal inflammation, paradoxic effects of this chemokine in relationship to retinal degeneration could also explain the complex of pathology observed in retinal degeneration and other neurodegenerative diseases.

Acknowledgments

We thank Drs. K. Palczewski, D. Mustafi, B. Kevany, Z. Dong, S. Howell (Case Western Reserve University), Y. Hirohashi (Sapporo Medical Univer-

sity, Sapporo, Japan), and T. Sakai (The Jikei University School of Medicine) for their comments and technical support.

Disclosures

The authors have no financial conflicts of interest.

References

1. Xu, H., M. Chen, and J. V. Forrester. 2009. Para-inflammation in the aging retina. *Prog. Retin. Eye Res.* 28: 348–368.
2. Kohno, H., Y. Chen, B. M. Kevany, E. Pearlman, M. Miyagi, T. Maeda, K. Palczewski, and A. Maeda. 2013. Photoreceptor proteins initiate microglial activation via Toll-like receptor 4 in retinal degeneration mediated by all-trans-retinal. *J. Biol. Chem.* 288: 15326–15341.
3. Mustafi, D., T. Maeda, H. Kohno, J. H. Nadeau, and K. Palczewski. 2012. Inflammatory priming predisposes mice to age-related retinal degeneration. *J. Clin. Invest.* 122: 2989–3001.
4. Shiose, S., Y. Chen, K. Okano, S. Roy, H. Kohno, J. Tang, E. Pearlman, T. Maeda, K. Palczewski, and A. Maeda. 2011. Toll-like receptor 3 is required for development of retinopathy caused by impaired all-trans-retinal clearance in mice. *J. Biol. Chem.* 286: 15543–15555.
5. Combadière, C., C. Feumi, W. Raoul, N. Keller, M. Rodéro, A. Pézard, S. Lavalette, M. Houssier, L. Jonet, E. Picard, et al. 2007. CX3CR1-dependent subretinal microglia cell accumulation is associated with cardinal features of age-related macular degeneration. *J. Clin. Invest.* 117: 2920–2928.
6. Ambati, J., A. Anand, S. Fernandez, E. Sakurai, B. C. Lynn, W. A. Kuziel, B. J. Rollins, and B. K. Ambati. 2003. An animal model of age-related macular degeneration in senescent Ccl-2- or Ccr-2-deficient mice. *Nat. Med.* 9: 1390–1397.
7. von Lintig, J., P. D. Kiser, M. Golczak, and K. Palczewski. 2010. The biochemical and structural basis for trans-to-cis isomerization of retinoids in the chemistry of vision. *Trends Biochem. Sci.* 35: 400–410.
8. Kiser, P. D., M. Golczak, A. Maeda, and K. Palczewski. 2012. Key enzymes of the retinoid (visual) cycle in vertebrate retina. *Biochim. Biophys. Acta* 1821: 137–151.
9. Allikmets, R., N. F. Shroyer, N. Singh, J. M. Seddon, R. A. Lewis, P. S. Bernstein, A. Peiffer, N. A. Zabriskie, Y. Li, A. Hutchinson, et al. 1997. Mutation of the Stargardt disease gene (ABCR) in age-related macular degeneration. *Science* 277: 1805–1807.
10. Allikmets, R., N. Singh, H. Sun, N. F. Shroyer, A. Hutchinson, A. Chidambaram, B. Gerrard, L. Baird, D. Stauffer, A. Peiffer, et al. 1997. A photoreceptor cell-specific ATP-binding transporter gene (ABCR) is mutated in recessive Stargardt macular dystrophy. *Nat. Genet.* 15: 236–246.
11. Janecke, A. R., D. A. Thompson, G. Utermann, C. Becker, C. A. Hübner, E. Schmid, C. L. McHenry, A. R. Nair, F. Rüschendorf, J. Heckenlively, et al. 2004. Mutations in RDH12 encoding a photoreceptor cell retinol dehydrogenase cause childhood-onset severe retinal dystrophy. *Nat. Genet.* 36: 850–854.
12. Quazi, F., S. Lenevich, and R. S. Molday. 2012. ABCA4 is an N-retinylidene-phosphatidylethanolamine and phosphatidylethanolamine importer. *Nat. Commun.* 3: 925.
13. Rattner, A., P. M. Smallwood, and J. Nathans. 2000. Identification and characterization of all-trans-retinol dehydrogenase from photoreceptor outer segments, the visual cycle enzyme that reduces all-trans-retinal to all-trans-retinol. *J. Biol. Chem.* 275: 11034–11043.
14. Maeda, A., T. Maeda, Y. Imanishi, V. Kuksa, A. Alekseev, J. D. Bronson, H. Zhang, L. Zhu, W. Sun, D. A. Saperstein, et al. 2005. Role of photoreceptor-specific retinol dehydrogenase in the retinoid cycle in vivo. *J. Biol. Chem.* 280: 18822–18832.
15. Maeda, A., T. Maeda, M. Golczak, S. Chou, A. Desai, C. L. Hoppel, S. Matsuyama, and K. Palczewski. 2009. Involvement of all-trans-retinal in acute light-induced retinopathy of mice. *J. Biol. Chem.* 284: 15173–15183.
16. Maeda, A., T. Maeda, M. Golczak, and K. Palczewski. 2008. Retinopathy in mice induced by disrupted all-trans-retinal clearance. *J. Biol. Chem.* 283: 26684–26693.
17. Gordon, S., and F. O. Martinez. 2010. Alternative activation of macrophages: mechanism and functions. *Immunity* 32: 593–604.
18. Mattapallil, M. J., E. F. Wawrousek, C. C. Chan, H. Zhao, J. Roychoudhury, T. A. Ferguson, and R. R. Caspi. 2012. The Rd8 mutation of the Crb1 gene is present in vendor lines of C57BL/6N mice and embryonic stem cells, and confounds ocular induced mutant phenotypes. *Invest. Ophthalmol. Vis. Sci.* 53: 2921–2927.
19. Wu, Y. P., and R. L. Proia. 2004. Deletion of macrophage-inflammatory protein 1 alpha retards neurodegeneration in Sandhoff disease mice. *Proc. Natl. Acad. Sci. USA* 101: 8425–8430.
20. Maeda, A., M. Golczak, Y. Chen, K. Okano, H. Kohno, S. Shiose, K. Ishikawa, W. Harte, G. Palczewska, T. Maeda, and K. Palczewski. 2011. Primary amines protect against retinal degeneration in mouse models of retinopathies. *Nat. Chem. Biol.* 8: 170–178.
21. Mainster, M. A., G. T. Timberlake, R. H. Webb, and G. W. Hughes. 1982. Scanning laser ophthalmoscopy. Clinical applications. *Ophthalmology* 89: 852–857.
22. Jung, S., J. Aliberti, P. Graemmel, M. J. Sunshine, G. W. Kreutzberg, A. Sher, and D. R. Littman. 2000. Analysis of fractalkine receptor CX(3)CR1 function by targeted deletion and green fluorescent protein reporter gene insertion. *Mol. Cell. Biol.* 20: 4106–4114.
23. Novak, M. L., and T. J. Koh. 2013. Macrophage phenotypes during tissue repair. *J. Leukoc. Biol.* 93: 875–881.
24. Liao, B., W. Zhao, D. R. Beers, J. S. Henkel, and S. H. Appel. 2012. Transformation from a neuroprotective to a neurotoxic microglial phenotype in a mouse model of ALS. *Exp. Neurol.* 237: 147–152.
25. Niederkorn, J. Y. 2006. See no evil, hear no evil, do no evil: the lessons of immune privilege. *Nat. Immunol.* 7: 354–359.
26. Cense, B., N. Nassif, T. Chen, M. Pierce, S. H. Yun, B. Park, B. Bouma, G. Tearney, and J. de Boer. 2004. Ultrahigh-resolution high-speed retinal imaging using spectral-domain optical coherence tomography. *Opt. Express* 12: 2435–2447.
27. Charbel Issa, P., H. J. Bolz, I. Ebermann, E. Domeier, F. G. Holz, and H. P. Scholl. 2009. Characterisation of severe rod-cone dystrophy in a consanguineous family with a splice site mutation in the MERTK gene. *Br. J. Ophthalmol.* 93: 920–925.
28. Seitz, H. M., T. D. Camenisch, G. Lemke, H. S. Earp, and G. K. Matsushima. 2007. Macrophages and dendritic cells use different Axl/Mertk/Tyro3 receptors in clearance of apoptotic cells. *J. Immunol.* 178: 5635–5642.
29. Nandrot, E. F., and E. M. Dufour. 2010. Mertk in daily retinal phagocytosis: a history in the making. *Adv. Exp. Med. Biol.* 664: 133–140.
30. Getts, D. R., R. L. Terry, M. T. Getts, M. Müller, S. Rana, B. Shrestha, J. Radford, N. Van Rooijen, I. L. Campbell, and N. J. King. 2008. Ly6c+ "inflammatory monocytes" are microglial precursors recruited in a pathogenic manner in West Nile virus encephalitis. *J. Exp. Med.* 205: 2319–2337.
31. Marques, C. P., M. C. Cheeran, J. M. Palmquist, S. Hu, S. L. Urban, and J. R. Lokensgard. 2008. Prolonged microglial cell activation and lymphocyte infiltration following experimental herpes encephalitis. *J. Immunol.* 181: 6417–6426.
32. Nahrendorf, M., F. K. Swirski, E. Aikawa, L. Stangenberg, T. Wurdinger, J. L. Figueiredo, P. Libby, R. Weissleder, and M. J. Pittet. 2007. The healing myocardium sequentially mobilizes two monocyte subsets with divergent and complementary functions. *J. Exp. Med.* 204: 3037–3047.
33. Kevany, B. M., and K. Palczewski. 2010. Phagocytosis of retinal rod and cone photoreceptors. *Physiology (Bethesda)* 25: 8–15.
34. Joly, S., M. Francke, E. Ulbricht, S. Beck, M. Seeliger, P. Hirrlinger, J. Hirrlinger, K. S. Lang, M. Zinkernagel, B. Odermatt, et al. 2009. Cooperative phagocytes: resident microglia and bone marrow immigrants remove dead photoreceptors in retinal lesions. *Am. J. Pathol.* 174: 2310–2323.
35. Engelhardt, B. 2008. Immune cell entry into the central nervous system: involvement of adhesion molecules and chemokines. *J. Neurol. Sci.* 274: 23–26.
36. Minagar, A., A. Carpenter, and J. S. Alexander. 2007. The destructive alliance: interactions of leukocytes, cerebral endothelial cells, and the immune cascade in pathogenesis of multiple sclerosis. *Int. Rev. Neurobiol.* 79: 1–11.
37. Cao, X., D. Shen, M. M. Patel, J. Tuo, T. M. Johnson, T. W. Olsen, and C. C. Chan. 2011. Macrophage polarization in the maculae of age-related macular degeneration: a pilot study. *Pathol. Int.* 61: 528–535.
38. Nussenblatt, R. B., and F. Ferris, III. 2007. Age-related macular degeneration and the immune response: implications for therapy. *Am. J. Ophthalmol.* 144: 618–626.
39. El Khoury, J., and A. D. Luster. 2008. Mechanisms of microglia accumulation in Alzheimer's disease: therapeutic implications. *Trends Pharmacol. Sci.* 29: 626–632.
40. Giunta, B., D. Obregon, R. Velisetty, P. R. Sanberg, C. V. Borlongan, and J. Tan. 2012. The immunology of traumatic brain injury: a prime target for Alzheimer's disease prevention. *J. Neuroinflammation* 9: 185.
41. Chen, M., J. V. Forrester, and H. Xu. 2011. Dysregulation in retinal para-inflammation and age-related retinal degeneration in CCL2 or CCR2 deficient mice. *PLoS ONE* 6: e22818.
42. Chan, C. C., R. J. Ross, D. Shen, X. Ding, Z. Majumdar, C. M. Bojanowski, M. Zhou, N. Salem, Jr., R. Bonner, and J. Tuo. 2008. Ccl2/Cx3cr1-deficient mice: an animal model for age-related macular degeneration. *Ophthalmic Res.* 40: 124–128.
43. Suzuki, M., M. Tsujikawa, H. Itabe, Z. J. Du, P. Xie, N. Matsumura, X. Fu, R. Zhang, K. H. Sonoda, K. Egashira, et al. 2012. Chronic photo-oxidative stress and subsequent MCP-1 activation as causative factors for age-related macular degeneration. *J. Cell Sci.* 125: 2407–2415.
44. Guo, C., A. Otani, A. Oishi, H. Kojima, Y. Makiyama, S. Nakagawa, and N. Yoshimura. 2012. Knockout of ccr2 alleviates photoreceptor cell death in a model of retinitis pigmentosa. *Exp. Eye Res.* 104: 39–47.
45. Ribeiro, S., and R. Horuk. 2005. The clinical potential of chemokine receptor antagonists. *Pharmacol. Ther.* 107: 44–58.
46. Cukras, C. A., P. Petrou, E. Y. Chew, C. B. Meyerle, and W. T. Wong. 2012. Oral minocycline for the treatment of diabetic macular edema (DME): results of a phase I/II clinical study. *Invest. Ophthalmol. Vis. Sci.* 53: 3865–3874.